Synthesis of Oxide Encapsulated and Freestanding Hydride Surface Terminated $Si_{1-x}Ge_x$ Nanocrystals

Eric J. Henderson and Jonathan G. C. Veinot*

Department of Chemistry, University of Alberta, Edmonton, Alberta T6G 2G2, Canada

Received January 4, 2007
Revised Manuscript Received March 6, 2007

Group IV semiconductor nanocrystals have long been the focus of intense research as a result of their unique chemical and optical characteristics.[1] The emergence of size dependent properties in nanoscale silicon and germanium has not only challenged semiconductor band structure models but also expanded the potential applications of these materials. Silicon and germanium nanocrystals (*nc*-Si, *nc*-Ge) both display size-dependent photoluminescence (PL)[2,3] resulting from quantum confinement effects. Because of their unique optical and electronic characteristics, these materials have been investigated for potential integration into a variety of optoelectronic[4,5] as well as data storage devices,[6] among others. It is well-established that alloying silicon with germanium affords a convenient method for tailoring the band gap energy of semiconductor thin films and bulk materials.[7] Since silicon and germanium form a continuous alloy throughout the entire compositional range, the alloy band gap energy can be monotonically tuned by increasing the germanium content. In this regard, silicon germanium alloy nanocrystals (*nc*-$Si_{1-x}Ge_x$), which also exhibit size-dependent PL,[8] could offer increased versatility relative to their elemental counterparts because their optical response can be tailored through compositional control.[9] These alloy nanocrystals have potential applications in thermophotovoltaics (TPV), tandem solar cells, and silicon-based optoelectronic devices.[7,10] Existing methods for preparing *nc*-$Si_{1-x}Ge_x$ include magnetron co-sputtering,[9−11] chemical vapor deposition (CVD),[7,12] thermal evaporation,[13] and molecular beam epitaxy (MBE),[14] all of which require subsequent high-temperature annealing. These infrastructure intensive fabrication methods only afford small quantities of oxide embedded or substrate supported nanocrystals. Current methods for preparing freestanding *nc*-$Si_{1-x}Ge_x$ also require elaborate equipment and experimental design while affording particles of ill-defined size and shape.[13,15]

Scheme 1. Thermally Induced Reactions Providing *nc*-$Si_{0.45}Ge_{0.55}$ from the Simultaneous Thermal Disproportionation of HSQ and GeI_2

$$HSQ\,(H_8Si_8O_{12}) \xrightarrow{350-500^\circ C} 6SiO_2 + 2SiH_4 \quad (1)$$

$$SiH_4 \xrightarrow{450^\circ C} Si + 2H_2 \quad (2)$$

$$2GeI_2 \xrightarrow{350^\circ C} Ge + GeI_4 \quad (3)$$

We recently reported the preparation of *nc*-Si from the thermally induced disproportionation of hydrogen silsesquioxane (HSQ).[16] We proposed that noncrystalline silicon nanodomains formed from the decomposition of silane originating from the collapse of the HSQ cage structure at 350−500 °C. These domains crystallized with heating above 900 °C. Germanium diiodide (GeI_2) disproportionates at 350 °C yielding elemental Ge and GeI_4.[17] Here we extend the versatility of our thermolytic method for synthesizing group IV semiconductor nanomaterials by preparing silicon−germanium alloy nanocrystals (*nc*-$Si_{0.45}Ge_{0.55}$) from the simultaneous thermal decomposition of HSQ and GeI_2. Unlike other *nc*-$Si_{1-x}Ge_x$ preparative methods that employ reagents requiring specialized handling procedures,[7,12] HSQ and GeI_2 are easily manipulated using standard laboratory techniques. Relevant decomposition reactions are summarized in Scheme 1.

Removal of the solvent from a FOx-17 (Dow Corning) HSQ stock solution in vacuo yields a white solid that was used without further purification. In a typical preparation, HSQ (0.20 g, 0.47mmol) and GeI_2 (1.60 g, 4.90mmol) were intimately mixed by mechanical grinding in a glovebox atmosphere to yield a uniform light yellow powder. The free flowing powder was transferred to a quartz reaction boat in a high-temperature tube furnace and heated to a maximum processing temperature of 1100 °C at approximately 60 °C/min in a slightly reducing atmosphere (5% H_2, 95% Ar). Reaction mixtures were heated for 1, 5, 10, and 20 h to yield GeI_4 and **1**, **2**, **3**, and **4**, respectively, as glassy brown solids (12% mass yield).

Sample **2** was ground into a fine powder and sonicated in a 5:1 mixture of H_2O_2:MeOH at 40 °C for 60 min to remove

* Corresponding author. E-mail: jveinot@ualberta.ca. Fax: 780-492-8231. Tel.: 780-492-7206.

(1) Canham, L. T. *Appl. Phys. Lett.* **1990**, *57* (10), 1046.
(2) Takeoka, S.; Fujii, M.; Hayashi, S.; Yamamoto, K. *Phys. Rev. B* **1998**, *58* (12), 7921.
(3) Veinot, J. G. C. *Chem. Commun.* **2006**, *40*, 4160.
(4) Pavesi, L.; Dal Negro, L.; Mazzoleni, C.; Franzò, G.; Priolo, F. *Nature* **2000**, *408*, 440.
(5) Kuo, Y. H.; Lee, Y. K.; Ge, Y.; Ren, S.; Roth, J. E.; Kamins, T. I.; Miller, D. A. B.; Harris, J. S. *Nature* **2005**, *437*, 1334.
(6) Compagnoni, C. M.; Gusmeroli, R.; Ielmini, D.; Spinelli, A. S.; Lacaita, A. L.; *J. Nanosci. Nanotechnol.* **2007**, *7*, 193.
(7) Palfinger, G.; Bitnar, B.; Sigg, H.; Müller, E.; Stutz, S.; Grützmacher, D. *Physica E* **2003**, *16*, 481.
(8) Weissker, H. C.; Furthmüller, J.; Bechstedt, F. *Phys. Rev. Lett.* **2003**, *90* (8), 085501-1.
(9) Takeoka, S.; Toshikiyo, K.; Fujii, M.; Hayashi, S.; Yamamoto, K. *Phys. Rev. B* **2000**, *61* (23), 15988.
(10) Yang, Y. M.; Wu, X. L.; Siu, G. G.; Huang, G. S.; Shen, J. C.; Hu, D. S. *J. Appl. Phys.* **2004**, *96* (9), 5239.
(11) Yang, Y. M.; Wu, X. L.; Yang, L. W.; Kong, F. *J. Cryst. Growth* **2006**, *291*, 358.
(12) Kling, A.; Ortiz, M. I.; Sangrador, J.; Rodríguez, A.; Rodríguez, T.; Ballesteros, C.; Soares, J. C. *Nucl. Instrum. Methods Phys. Res., Sect. B* **2006**, *249*, 451.
(13) Lin, C. W.; Lin, S. Y.; Lee, S. C.; Chia, C. T. *J. Appl. Phys.* **2002**, *91* (4), 2322.
(14) Tang, Y. S.; Cai, S.; Jin, G.; Duan, J.; Wang, K. L.; Soyez, H. M.; Dunn, B. S. *Appl. Phys. Lett.* **1997**, *71* (17), 2448.
(15) Liao, Y. C.; Lin, S. Y.; Lee, S. C.; Chia, C. T. *Appl. Phys. Lett.* **2000**, *77* (26), 4328.
(16) Hessel, C. M.; Henderson, E. J.; Veinot, J. G. C. *Chem. Mater.* **2006**, *18* (26), 6139.
(17) Cronemeyer, D. C. *J. Appl. Phys.* **1958**, *29* (12), 1730.

10.1021/cm070022l CCC: $37.00
Published on Web 03/22/2007

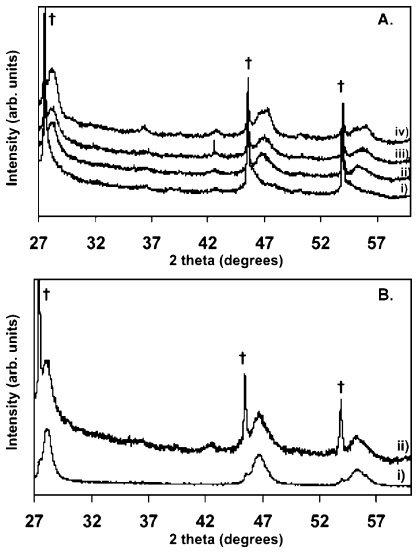

Figure 1. (A) XRD patterns obtained for (i) **1**, (ii) **2**, (iii) **3**, and (iv) **4**, showing the characteristic (111), (220), and (311) reflections of *nc*-$Si_{0.45}Ge_{0.55}$. (B) XRD patterns obtained for (i) **5** and (ii) **2**. († denote reflections arising from bulk Ge impurities.)

bulk Ge and GeI_4 impurities.[18] After the powder was isolated by centrifugation and dried in an argon stream, hydride surface terminated *nc*-$Si_{0.45}Ge_{0.55}$ molecules were liberated from the oxide matrix upon etching with hydrofluoric acid (HF) ethanol−water solutions for 60 min and isolated as an ultrafine black powder, **5**, using repeated centrifugation/sonication cycles in deionized water.

Bulk crystallinity of oxide encapsulated and freestanding *nc*-$Si_{0.45}Ge_{0.55}$ was evaluated by X-ray diffraction (XRD) using an INEL XRG 3000 X-ray diffractometer equipped with a Cu Kα radiation source. The bonding within the *nc*-$Si_{0.45}Ge_{0.55}$ core was investigated by Raman spectroscopy using a Renishaw inVia Raman microscope equipped with a 785 nm diode laser and a power of 7.94 mW on the sample. Bonding was further investigated by Fourier transform infrared spectroscopy (FTIR) using a Nicolet Magna 750 IR spectrophotometer. Crystal morphology, size distribution, and chemical composition were evaluated by transmission electron microscopy (TEM) and energy dispersive X-ray spectroscopy (EDX) using a JEOL-2010 (LaB_6 thermionic emission source) electron microscope with an accelerating voltage of 200 keV. TEM samples of freestanding *nc*-$Si_{0.45}Ge_{0.55}$ were drop-coated from a clear brown methanol suspension onto a carbon coated copper grid.

Influence of annealing time was monitored using XRD (Figure 1A). After 1 h, **1**, only sharp peaks corresponding to bulk diamond lattice Ge can be definitively assigned. These bulk Ge impurities result from Ge crystallization outside of the SiO_2-like matrix that forms with HSQ decomposition. Weak, broad reflections appearing as shoulders on the bulk Ge reflections are also observed for **1**; however, it is nearly impossible to make a definitive assignment. XRD patterns of **2**−**4** (Figure 1A) clearly show broad diffraction peaks appearing at approximately $2\theta = 28°$, 47°, and 55° which are readily indexed to characteristic (111), (220), and

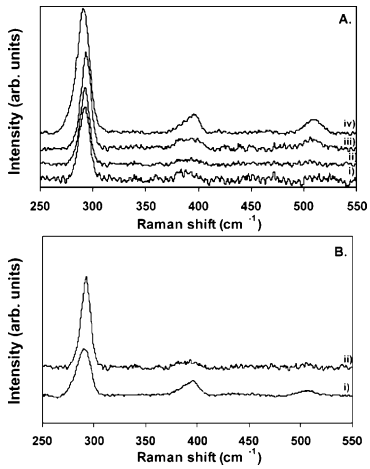

Figure 2. (A) Raman spectra obtained for (i) **1**, (ii) **2**, (iii) **3**, and (iv) **4**, showing the Ge−Ge, Si−Ge, and Si−Si OP vibrations characteristic of *nc*-$Si_{0.45}Ge_{0.55}$. (B) Raman spectra for (i) **5** and (ii) **2**.

(311) reflections of diamond lattice $Si_{0.45}Ge_{0.55}$. Figure 1A shows the diffraction peaks do not shift in **2**, **3**, and **4**, highlighting the elemental composition of the alloy remains constant regardless of thermal processing time. The experimentally determined alloy lattice constant (5.526 Å)[19] was used to estimate the alloy composition as $Si_{0.45}Ge_{0.55}$ using (eq 4),

$$a(x) = 0.002\,733x^2 + 0.019\,92x + 0.5401\ \text{nm} \qquad (4)$$

where a is the lattice constant and x is the Ge mole fraction.[20]

We also note that *nc*-$Si_{0.45}Ge_{0.55}$ reflection intensities in the XRD patterns of **2**−**4** qualitatively increase with extended heating. Similar time dependent intensity relationships observed for $Si_{1-x}Ge_x$ have been attributed to increased particle crystallinity.[21] The XRD patterns of **2**−**4** exhibit peak broadening independent of annealing time, suggesting a constant nanoparticle size. The Debye−Scherrer relationship affords an estimated nanocrystal diameter of 6.8 nm for **2**−**4**. Figure 1B shows XRD patterns for **2** and **5**, *nc*-$Si_{0.45}Ge_{0.55}$ liberated from the oxide matrix through HF etching of **2**. It is clear that the (111), (220), and (311) reflections for **5** are consistent with the patterns obtained for **2**. Figure 1B also shows a dramatic decrease in the intensity of bulk Ge reflections after the liberation process. Residual bulk Ge is likely the result of incomplete etching. It is clear that the liberated *nc*-$Si_{0.45}Ge_{0.55}$ molecules maintain crystallinity and a constant composition throughout the etching process.

Figure 2A shows baseline corrected Raman spectra for **1**−**4**. Each spectrum shows asymmetric peaks at approximately 292, 395, and 507 cm^{-1}, corresponding to vibrations of the Ge−Ge, Si−Ge, and Si−Si optical phonons (OP), respectively. As expected, the Ge−Ge OP vibration is the most intense because of the bulk Ge impurities identified in the XRD patterns. It is clear that prolonged annealing increases the intensities of the OP vibrations characteristic

(18) Premak, W.; Kampworth, R.; Dayal, Y. *J. Electrochem. Soc.* **1967**, *114*, 88.

(19) See ref 13 for lattice constants for Si = 0.534 nm and Ge = 0.566 nm.

(20) Yang, Y. M.; Wu, X. L.; Huang, G. S.; Hu, D. S.; Siu, G. G. *Phys. Lett. A* **2005**, *338*, 379.

(21) Hwang, C. W.; Ryu, M. K.; Kim, K. B.; Lee, S. C.; Kim, C. S. *J. Appl. Phys.* **1995**, *77* (7), 3042.

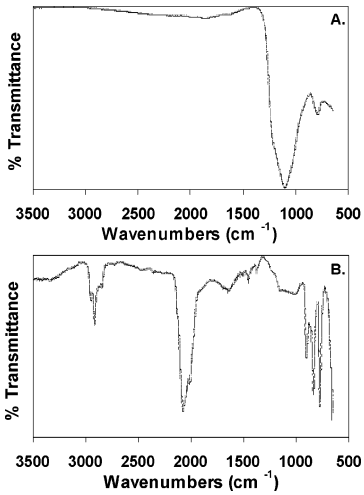

Figure 3. (A) FTIR spectrum of **2**. (B) FTIR spectrum obtained for **5**, showing Si−H_x and Ge−H_x stretches and scissoring.

of *nc*-$Si_{0.45}Ge_{0.55}$. This can be related to an increase in the number of Ge−Ge, Si−Ge, and Si−Si bonds, consistent with the XRD data that suggest increased particle crystallinity upon extended annealing. Figure 2B shows baseline corrected Raman spectra for **2** and **5**. The Raman spectrum of **5** shows a decrease in the Ge−Ge OP vibration intensity and an increase in the intensity of Si−Ge and Si−Si vibrations, consistent with the removal of the bulk Ge impurities during the liberation procedure. Shifts in the Raman frequencies of *nc*-$Si_{1-x}Ge_x$ with respect to bulk Si and bulk Ge can be related to elemental composition, phonon confinement effects, particle size, and stress relaxation of matrix embedded particles.[10] However, particle size and composition are not readily obtained through the Raman data because it is nontrivial to distinguish between these factors and their relative contributions to the overall shift.

Figure 3 shows the FTIR spectra of **2** and **5**. The FTIR spectrum of **2** (Figure 3A) is dominated by a broad band associated with Si−O−Si bending (ca. 1100 cm^{-1}) of the SiO_2-like matrix. Upon etching with HF acid, **5** (Figure 3B), the oxide is removed and the nanocrystal surface is dominated by Si−H and Ge−H functionalities, as evidenced by the vibrations at approximately 2100 cm^{-1} (Si−H_x and Ge−H_x stretches). Bending frequencies of Si−O−Si bonding at $\leq$1400 cm^{-1} remain, suggesting the presence of a small amount of surface oxide possibly arising from incomplete etching and post-etching oxidation of the nanocrystal surface. Further evidence for hydride surface termination are the peaks at $\leq$1000 cm^{-1} assigned to Si−H_x and Ge−H_x scissoring. Peaks appearing at approximately 2900 cm^{-1} and 1500−1400 cm^{-1} are from residual ethanol used in the etching process. Hydride terminated nanocrystal surfaces have been shown to act as reaction platforms for the formation of Si−C and Ge−C bonds via hydrosilylation and hydrogermylation reactions, respectively.[3,22]

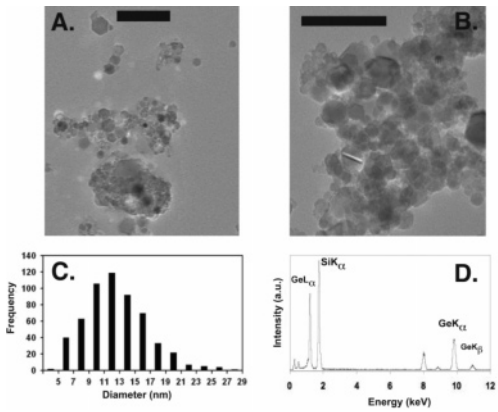

Figure 4. (A, B) Representative bright field TEM micrographs of **5** (bar = 100 nm). (C) Size distribution of **5** (mean = 12.68 nm, 2σ = 4.09 nm, n = 565). (D) EDX spectrum of **5**.

Images A and B of Figure 4 show representative bright-field TEM images of freestanding *nc*-$Si_{0.45}Ge_{0.55}$, **5**. Many of the nanocrystals have aggregated, most likely resulting from hydrophobic interactions between the hydride surface terminated nanocrystals and water impurities in the methanol suspension. It can be seen that the nanocrystals adopt pseudospherical morphologies. Figure 4C shows the measured size distribution with a mean diameter of 12.68 nm (2σ = 4.09 nm; n = 565). This value differs significantly from the value determined using Scherrer analysis. Inhomogeneous strain within the nanocrystals resulting from alloying defects and crystal lattice mismatches could cause an increase in XRD signal broadening and account for the small crystal size calculated from the Scherrer analysis.[23] Lattice spacings determined using selected area electron diffraction are consistant with XRD and support a Si:Ge ratio of 0.45:0.55. Figure 4D shows the EDX spectrum of liberated *nc*-$Si_{0.45}Ge_{0.55}$, showing the nanocrystals are composed only of Si and Ge.

In summary, we report the preparation of pseudospherical $Si_{0.45}Ge_{0.55}$ alloy nanocrystals via the simultaneous thermally induced disproportionation of HSQ and GeI_2. XRD suggested a composition consistent with $Si_{0.45}Ge_{0.55}$ that remained constant regardless of annealing time and HF etching. XRD, Raman spectroscopy, TEM, and EDX all confirm the presence of *nc*-$Si_{0.45}Ge_{0.55}$. FTIR spectroscopy confirmed nanoparticle hydride surface termination upon HF etching. Ongoing investigations include tailoring of particle shape, size, composition, and surface chemistry as well as an investigation of the PL response of these materials.

Acknowledgment. C.W. Moffat and R. Lister are thanked for assistance with FT-IR. Prof. M. Dermott and N. Yang are thanked for assistance with Raman spectroscopy. C. Hessel is thanked for useful discussions and assistance with TEM imaging. S. McFarlane, D. Rollings, and J. Kelly are also thanked for useful discussions. The University of Alberta and NSERC are thanked for funding.

CM070022L

(22) Fok, E.; Shih, M.; Meldrum, A.; Veinot, J. G. C. *Chem. Commun.* **2004**, *10*, 386.

(23) Tian, H. H.; Atzmon, M. *Philos. Mag. A* **1999**, *79* (8), 1769.